

# An improved localization method in cyber-social environments with obstacles<sup>☆</sup>



Zhigang Gao<sup>a,\*</sup>, Hongyi Guo<sup>a</sup>, Yunfeng Xie<sup>a</sup>, Huijuan Lu<sup>b</sup>, Jianhui Zhang<sup>a</sup>, Wenjie Diao<sup>a</sup>, Ruichao Xu<sup>a</sup>

<sup>a</sup> College of Computer Science and Technology, Hangzhou Dianzi University, Hangzhou, China

<sup>b</sup> College of Information Engineering, China Jiliang University, Hangzhou, China

## ARTICLE INFO

### Article history:

Received 30 November 2018

Revised 21 August 2019

Accepted 30 April 2020

### Keywords:

Cyber-Social Systems

WiFi-Based localization

Angle of Arrival (AOA)

Unscented Kalman filter

## ABSTRACT

In Cyber-Social Systems (CSS), sensors play a key role in the intelligent perception and recognition of people, objects and the environments, in which target localizing is one of the important issues. It is often difficult to accurately and conveniently localize the sensors due to the presence of Non-Line Of Sight (NLOS) when there are obstacles. This paper proposes a sensor localization method based on WiFi (Wireless Fidelity) localization, which first collects the angle and intensity information of the WiFi signals of mobile base stations during a linear or curvilinear motion, then uses the Nonlinear Inequality Constrained-Unscented Kalman Filter (NIC-UKF) method presented in this paper to filter interference, so as to localize the positions of sensors. The method has stronger stability, high precision, and acceptable computing overhead, which is suitable for the localization of fixed or low-speed moving targets in Cyber-Social environments with obstacles.

© 2020 Elsevier Ltd. All rights reserved.

## 1. Introduction

At present, with the rapid development of network technology and sensing technology, Cyber-Physical Systems (CPS) have become more and more popular [1–3]. CPS integrate computing, communication, and control, and it changes the interaction way between people and the real world by merging the cyber world and the physical world. As the Internet of Things (IoT) plays an increasingly important role in human activity, CSS, combined with social computing and sensing computing, have attracted many researchers' attention [4]. CSS acquire information about human society through IoT systems, including environments, transportation, and social activities, to optimize people's interactions and social management. In CSS, location information is widely used. For example, in location-based social networking APPS (APPLICATIONS), social networking APPS recommend new friends to users based on their geographic location information; in advertisement APPS, service providers push advertisement in a timely manner based on the environments and locations of users; and in some open wilderness or complex indoor parks, the locations of persons need to be probed to provide the corresponding guiding service. Therefore, it is important to determine the locations of the wireless nodes deployed on objects or persons.

For decades, there are many research works to estimate the locations of wireless nodes without using GPS modules [5,15–21]. In CSS, many activities occur in environments such as in mountains, shopping malls, and indoor meeting places,

<sup>☆</sup> This paper is for CAEE special section SI-csc Reviews processed and recommended for publication to the Editor-in-Chief by Guest Editor Dr. Xiaokang Zhou.

\* Corresponding author.

E-mail address: [gaozhigang@hdu.edu.cn](mailto:gaozhigang@hdu.edu.cn) (Z. Gao).

etc., where 3G/4G or GPS signals are weak because the transmission of wireless signals is blocked by obstacles. How to localize the wireless nodes accurately in those environments is an important prerequisite for the effectively work of CSS. When there are obstacles, wireless node localization will incur additional errors due to the presence of NLOS. A challenging problem is how to mitigate the impact of NLOS [6]. A common strategy in NLOS mitigation techniques is to use filtering approaches, e.g., the Kalman filter [7–8], the Extended Kalman Filter (EKF) [9–10], the Unscented Kalman Filter (UKF) [9,11], and the Particle Filter (PF) [12]. In order to deal with the nonlinear models of localization problems in CSS, some researches linearize the nonlinear models by using linearization techniques [13–14]. However, linearization techniques will incur some performance degradation in localization accuracy. In addition, nonlinear filters such as EKF, UKF and PF will also suffer from the problem of filtering divergence [14]. To the best of our knowledge, few studies have focused on filtering divergence of nonlinear filters.

In this paper, we propose a localization method based on WiFi signals, which first collects the angle and intensity information of WiFi signals of mobile base stations, and then uses NIC-UKF to filter the signals, so as to localize the positions of sensors. The main contribution of this paper is that we present the NIC-UKF method to solve the problem of filtering divergences, and NIC-UKF can effectively mitigate the impact of NLOS. Furthermore, we present the method of extending the motion trajectory of a mobile base station to curvilinear motions, making NIC-UKF more suitable to the real-world applications.

The remainder of this paper is organized as follows. In Section 2, we introduce the related work on wireless node localization. In Section 3, we describe the application scenario and ranging models. In Section 4, we present the NIC-UKF method in detail. Experimental results and analyses are performed in Section 5. Finally, Section 6 summarizes this paper.

## 2. Related work

### 2.1. Wireless node localization

There are two kinds of algorithms about wireless node localization in CSS, i.e., range-free localization algorithms [5,15–16] and range-based localization algorithms [17–20]. Range-free localization algorithms depend on hardware devices and use network connectivity to estimate the approximate distance. Range-based localization algorithms estimate the distance between unknown nodes and base stations by ranging, which is usually calculated based on Received Signal Strength Indication (RSSI), Time Of Arrival (TOA), Time Difference Of Arrival (TDOA), or AOA.

Aiming at range-free localization algorithms, Zhou et al. proposed an improved APIT (Approximation Point-In-Triangulation) range-free localization algorithm which expands the definition of neighbor nodes and imports neighbor legality to improve the accuracy of localization estimation [5]. By introducing the weight of anchor nodes, Li et al. proposed a weighted DV-Hop (Distance Vector Hop) algorithm [21], and Wang et al. proposed a weighted centroid localization algorithm [15] to improve the localization accuracy. Sun et al. proposed an improved MDS-MAP (MultiDimensional Scaling MAP) algorithm which reduced distance matrix involved and fully used nodes with ranging capability to reduce computational complexity [16].

Aiming at range-based localization algorithms, the Whistle algorithm designed by Xu et al. fundamentally changes TDOA in the sense of relaxing the synchronization requirement and avoiding the error caused by time synchronization [17]. Leng et al. proposed an improved RSSI filter based on the reference distance to reduce the RSS fluctuation [18]. Pradhan et al. proposed a line intersection algorithm named the advanced TOA to solve the problem of TOA fluctuation [19]. Zhang et al. proposed a new approach named the AOA based Three-dimensional Multi-target Localization (ATML) to solve the problem of multiple sensor nodes localization under the 3D condition [20].

With the improvement of device accuracy, the range-based localization algorithm exhibits more advantage, such as higher accuracy and stronger flexibility. However, single measurement approach will incur measurement errors inevitably. In this paper, we adapt a method combining RSSI with AOA to get more accurate locations.

### 2.2. NLOS mitigation techniques

NLOS mitigation techniques are big challenges in wireless node localization due to the obstacles in the direct propagation paths of signals. NLOS will lead to unreliable localization and significantly reduce the localization accuracy if its impact is not properly dealt with.

It is a low-cost and effective approach to eliminate the errors of NLOS by filtering. Zhang et al. proposed a NLOS error mitigation algorithm based on the Kalman filter. Both the true values of TOA and the NLOS errors are served as the state variance of the Kalman filter [8]. To simplify the process of nonlinear models, some researchers use linearized techniques to address the nonlinear problem. Khan et al. first linearized the nonlinear model by employing RSSI/AOA, and then applied the Kalman filter to localizing the positions of wireless nodes [13]. Tomic et al. proposed an approach based on maximizing a posteriori principle and a Kalman filter to linearize the nonlinear problem of target tracking by converting coordinate system from the cartesian coordinate to the polar coordinate [14]. In addition, EKF, UKF and PF also can be used to solve the nonlinear problem. Hammes et al. proposed a robust EKF for tracking a mobile node based on semi-parametric estimators [10]. Nowak and Eidloth proposed an approach to overcome the multipath problem by using UKF dynamically to estimate the channel states [11]. Read et al. proposed a distributed PF for nonlinear tracking problem in Wireless Sensor Networks



Fig. 1. The application scenario of NIC-UKF.

(WSN). When using the same number of particles as a centralized filter, the speed of the distributed PF algorithm is four times faster than that of PF [12].

In this paper, because UKF has a good performance in dealing with nonlinear measurement models, we select UKF to mitigate the impact of NLOS. But UKF suffers from possible filtering divergence at the beginning of filtering process. We overcome this problem by presenting the NIC-UKF method.

### 3. Application scenario and ranging models

In this section, we first introduce the application scenario of NIC-UKF in Section 3.1, and then we describe the ranging model that will be used in the following sections in Section 3.2 and Section 3.3. Finally, we define the constraints used in NIC-UKF.

#### 3.1. Application scenario

In this paper, the application scenario is shown in Fig. 1. In Fig. 1, the sensor nodes are randomly deployed in the wild, and their deployment locations are uncertain in advance and may be shielded by trees, stones, or walls, etc. In order to measure the positions of the wireless sensors, a vehicle carrying a WiFi mobile base station travels on the road once and measures the signals of each node at certain intervals. For each sensor node, its angle and WiFi strength information is measured in three or more different positions, and its position can be determined by using the NIC-UKF method. Note that this scenario can also be extended to indoor ones, and the mobile base station can also be any device with the ability to measure the strength and angle information of WiFi signals.

#### 3.2. RSSI ranging model

RSSI ranging is used to estimate the distance based on the attenuation characteristics of the signal transmission process. The distance between two points can be calculated according to the RSSI power value between the transceivers and the signal transmission model.

In wireless transmission, the existing propagation path loss models include the free space propagation model, the log-distance path loss model, the hata model and the log-distance distribution model, etc [22]. In this paper, we select the log-distance path loss model because it can meet the requirements of diverse real-world environments.

The log-distance path loss model consists of two parts. The first part is the path loss after transmitting a certain distance, which can be used to predict the average power received in a distance  $d_i$ . The second part is the Gaussian random variable. The RSSI value at  $d_i$  is

$$P(d_i) = P_T + G - PL(d_0) - 10\epsilon \lg \left( \frac{d_i}{d_0} \right) - W_\sigma \quad (1)$$

Where  $P(d_i)$  represents the RSSI value of the wireless node  $i$  received by the base station,  $P_T$  represents the signal transmission power,  $G$  represents the antenna gain;  $PL(d_0)$  represents the path loss of the reference distance  $d_0$  (usually  $d_0=1\text{m.}$ ), and  $d_i$  represents the distance between a node  $i$  and the base station;  $\epsilon$  represents the signal loss attenuation factor relevant to the environment.  $W_\sigma$  represents a Gaussian distribution random variable with a mean of zero ( $\sigma$  is usually set to 4–6). In the right side of Eq. (1),  $W_\sigma$  is the Gaussian random variable, and the other part is path loss.

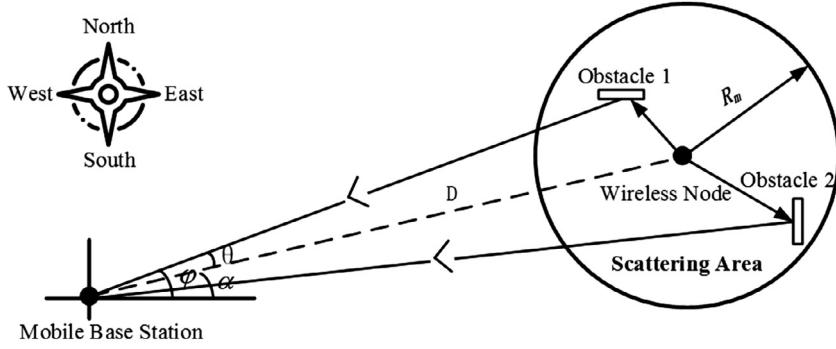


Fig. 2. Parameters in GBSBSCM.

Let  $\gamma = P_T + G - PL(d_0) - W_\sigma$ , thus the distance  $d_i$  can be denoted as

$$d_i = 10^{\frac{\gamma - P(d_i)}{10\epsilon}} \quad (2)$$

### 3.3. Geometrically Based Single Bounce Statistics Channel Model (GBSBSCM)

GBSBSCM is a single-channel model used in AOA localization algorithms, which is suitable for the micro-cellular environment. In this paper, we assume the height of base station antennas is higher than that of wireless nodes.

As shown in Fig. 2, obstacles are distributed in a circle whose center is the wireless node to be localized.  $\varphi$  represents the angle between the obstacle 1 and the East orientation;  $\alpha$  represents the angle between the East orientation and the wireless node; and  $\theta$  represents the angle between the wireless node and the obstacle 1.  $R_m$  is the radius of obstacles which have influence on the localization of the mobile base station. The distance  $D$  between the wireless node and the mobile base station is greater than  $R_m$ .

In Fig. 2, the maximum delay spread  $\tau_{\max}$  and the maximum angle spread  $\theta_{\max}$  are defined as

$$\begin{aligned} \tau_{\max} &= 2R_m/c \\ \theta_{\max} &= \arcsin\left(\frac{R_m}{D}\right) = \arcsin\left(\frac{R_m}{\sqrt{(x-x_i)^2 + (y-y_i)^2}}\right) \end{aligned} \quad (3)$$

where  $c$  is the speed of light. When the location of the mobile base station is known, the maximum delay spread and the maximum angular spread are only related to the size of the scattering area. The radius  $R_m$  of the scattering region can be derived from actual measurement or the COST-207 model [23].

In this paper, we use the RSSI ranging model to model the strength of WiFi signals, and GBSBSCM to localize the positions of wireless nodes. So we use the same parameters in the two models. However, the RSSI measurement value will generate a positive error due to the presence of NLOS. As a result, the RSSI measurement value will increase and the prediction distance between a wireless node and a base station will decrease. In order to solve the above problem, after we get the maximum angle spread  $\theta_{\max}$  through GBSBSCM, we consider the values of RSSI and AOA subject to the constraints as follows.

$$\text{st.} \begin{cases} \theta_{\max} - (\varphi - \alpha) \geq 0 \\ d_i - 10^{\frac{\gamma - P(d_i)}{\epsilon}} \geq 0 \end{cases} \quad (4)$$

## 4. Implementation process of NIC-UKF

NIC-UKF includes four phases, i.e., the initialization phase, the unscented transformation (UT) phase, the prediction phase, and the update phase. The flow of NIC-UKF is shown in Fig. 3.

The purpose of the initialization phase is to determine the object Eq. and the observation Eq., and to initialize the required parametric vectors, such as the state vector, the state transfer matrix and the covariance matrix of the noise. The purpose of the unscented transformation phase is to carry out data fusion. If there are the current measurement value (the RSSI and angle values measured by the receiving device) and the estimation of the previous period, the unscented transformation can estimate the current state vector, which can be considered to be a reliable optimal estimation of the state value. The purpose of the prediction phase is to predict the state of the  $(k+1)$ -th moment by using the estimation of the  $k$ -th moment state. The purpose of the update phase is to obtain the optimal estimation of the state vector of the  $(k+1)$ -th moment according to the target Eq. and the observation Eq., together with the measurement value of the  $k$ -th moment and the estimation value of the  $(k+1)$ -th moment.

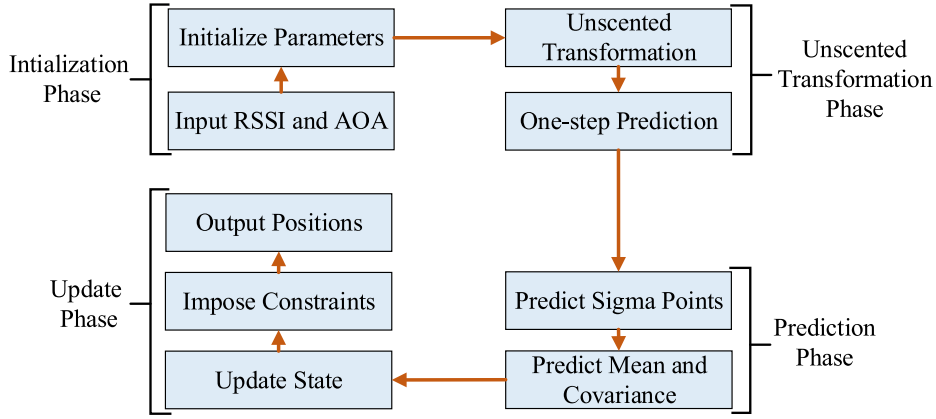


Fig. 3. The flow of NIC-UKF.

#### 4.1. Initialization phase

In UKF, nonlinear functions consist of an objective Eq.  $X$  with Gaussian noise  $W_k$  and an observation Eq.  $Z$  with Gaussian noise  $V_k$ , as defined in

$$\begin{cases} X_{k+1} = f(x_k, W_k) \\ Z_k = h(x_k, V_k) \end{cases} \quad (5)$$

In Eq. (5), the objective Eq. reflects the state change process of the base station when it moves from the location of the  $k$ -th moment to the one of the  $(k+1)$ -th moment. The observation Eq. represents the observation estimation value calculated by the state vector. For example, given the distance between a moving base station and a wireless node, we can calculate the estimated RSSI value by the observation Eq.. However, in the NLOS propagation environment, both the estimated RSSI value and the measured RSSI value have errors. The unscented Kalman filter comprehensively considers the measured value and the estimated value, and obtains the RSSI value close to the real-world environment after many rounds of iteration and the optimal estimation. The objective function in (5) is defined as

$$X_{k+1} = \Phi X_k + W_k \quad (6)$$

We assume the movement trajectory of the mobile base station is a uniform linear motion. We define the state vector  $X$  as

$$X = (x, v_x, y, v_y, \tan \alpha) \quad (7)$$

where  $(x, y)$  represents the location of mobile base station,  $v_x$  and  $v_y$  represent the velocities in the  $x$  and  $y$  directions respectively,  $\alpha$  represents the angle between the mobile base station and the wireless node. We assume  $\Delta t$  represents the sampling period. The state-transition matrix  $\Phi$  is defined as

$$\Phi = \begin{bmatrix} 1 & \Delta t & 0 & 0 & 0 \\ 0 & 1 & 0 & 0 & 0 \\ 0 & 0 & 1 & \Delta t & 0 \\ 0 & 0 & 0 & 1 & 0 \\ 0 & 0 & 0 & \frac{\Delta t}{x_k} & \frac{x_{k-1}}{x_k} \end{bmatrix} \quad (8)$$

We assume  $y_{k-1}$  represents the position of mobile base station in the  $y$  direction at the previous moment. According to the distance evaluated from RSSI and AOA and an anti-trigonometric Eq., we define the observation Eq. in Eq. (5) as

$$Z_k = h(X_k) + V_k = \begin{bmatrix} \arctan\left(\frac{y_k - y}{x_k - x}\right) \\ -10\epsilon \lg\left(\sqrt{(x_k - x)^2 + (y_k - y)^2} + \gamma\right) \end{bmatrix} + V \quad (9)$$

Where  $h(X_k)$  is the observation value, and  $V$  is the noise of the observation value. In Eq. (9), the observation Eq. is nonlinear, so we use the unscented Kalman filter to deal with the nonlinear problems. The purpose of Sigma sample points in the unscented Kalman filter is to deal with the nonlinear transfer problem of mean and covariance, and to approximate the probability density function of the state vectors by a series of Sigma sample points that conform to the original state distribution. The mean and covariance after the nonlinear transformation can obtain at least the 3-order precision of Taylor expansion.

We assume that the activation noise  $W_k$  has a covariance matrix  $Q$  and the measurement noise  $V_k$  has a covariance matrix  $R$ . The filter can get better performance by searching the optimal  $Q$  through experiments.  $Q$  is a diagonal matrix

generally with very small values of the main diagonal, so it is easy to converge quickly. The value of  $R$  is related to the precision of the measuring instrument. Similar to  $Q$ ,  $R$  can be obtained through experiments. The smaller the value of  $R$ , the faster the speed of convergence.  $Q$  and  $R$  are defined as

$$Q = \begin{bmatrix} 1 & 0 & 0 & 0 & 0 & 0 \\ 0 & 1 & 0 & 0 & 0 & 0 \\ 0 & 0 & 0.1^2 & 0 & 0 & 0 \\ 0 & 0 & 0 & 0.1^2 & 0 & 0 \\ 0 & 0 & 0 & 0 & 0.01^2 & 0 \\ 0 & 0 & 0 & 0 & 0 & 0.01^2 \end{bmatrix}, R = \begin{bmatrix} 5^2 & 0 \\ 0 & 0.01^2 \end{bmatrix} \quad (10)$$

In the initialization phase, we need to input the value of RSSI and AOA. Furthermore, we initialize the parameters such as  $\mathbf{X}_0$ ,  $\mathbf{Z}_0$ ,  $\Phi$ ,  $Q$  and  $R$ .

#### 4.2. Unscented transformation phase

UKF uses a sampling technique named as the unscented transformation to meet the mean and covariance of nonlinear problems. In the unscented transformation phase, UKF first selects some sample points according to a certain rule in the original state distribution. It requires the mean and covariance of sample points are equal to those of the original state distribution. After that, these sample points are substituted into the nonlinear functions to obtain the corresponding transformed mean and covariance. The transformed mean and covariance have the third-order Taylor expansion accuracy for Gaussian distribution. The state vector  $\mathbf{X}$  of Eq. (7) is an  $n$ -dimensional variable, and its mean  $\bar{\mathbf{X}}$  and variance  $\mathbf{P}$  are known. The formulas for calculating the  $2n+1$  Sigma sample points  $\mathbf{X}$  are defined as

$$\begin{cases} \mathbf{X}(0) = \bar{\mathbf{X}}, i = 0 \\ \mathbf{X}(i) = \bar{\mathbf{X}} + (\sqrt{(n+\lambda)\mathbf{P}}), i = 1 \sim n \\ \mathbf{X}(i) = \bar{\mathbf{X}} - (\sqrt{(n+\lambda)\mathbf{P}}), i = n+1 \sim 2n \end{cases} \quad (11)$$

where  $(\sqrt{\mathbf{P}_x})^T (\sqrt{\mathbf{P}_x}) = \mathbf{P}_x$ , and the variance  $\mathbf{P}_x$  is the  $x$ -th state vector of  $\mathbf{X}$ . The corresponding weights of these sample points are defined as

$$\begin{cases} \omega_m(0) = \frac{\lambda}{n+\lambda} \\ \omega_c(0) = \frac{\lambda}{n+\lambda} + (1 - a^2 + \beta) \\ \omega_m(i) = \omega_c(i) = \frac{\lambda}{2(n+\lambda)}, i = 1 \sim 2n \end{cases} \quad (12)$$

where  $\omega$  represents the relevant weight of sample points,  $m$  denotes the mean of sample points,  $c$  denotes the covariance of sample points,  $i$  is the number of sample points ( $i = 1, 2, \dots, 2n+1$ ), and  $\lambda$  is a scaling parameter used to reduce the total prediction error ( $\lambda = a^2(n + \kappa) - n$ ). The selection of the parameter  $a$  controls the distribution state of the sample points.  $\kappa$  is a pending parameter. Although there is no limitation for the value of  $\kappa$ , it should usually ensure that the matrix  $(n + \lambda)\mathbf{P}$  is a positive semidefinite matrix. The pending parameter  $\beta$  is a non-negative weight coefficient, it can combine the moment of the high order Taylor expansion to meet the nonlinear requirements.

#### 4.3. Prediction phase

After obtaining a set of Sigma points in the unscented transformation phase, we calculate the corresponding weights of  $\mathbf{X}_k(i)$  (i.e., the  $i$ -th column of the Sigma point set  $\mathbf{X}$  at the time moment  $k$ .) by

$$\mathbf{X}_k(i) = \left[ \hat{\mathbf{X}}_k \hat{\mathbf{X}}_k + \sqrt{(N+\lambda)\mathbf{P}(k)} \hat{\mathbf{X}}_k - \sqrt{(N+\lambda)\mathbf{P}_k} \right] \quad (13)$$

where  $\hat{\mathbf{X}}_k$  represents the estimation state vector at the time moment  $k$ , and then we calculate  $\mathbf{X}_{k+1}^-(i)$  (i.e., the one-step prediction of the  $i$ -th sampling point of Sigma point set  $\mathbf{X}$  at the time moment  $k+1$ ) by

$$\mathbf{X}_{k+1}^-(i) = f[k, \mathbf{X}_k(i)] \quad (14)$$

In the following part, the superscript "-" denotes the prediction value, and the superscript "^" denotes the estimation value. In Eq. (14), the purpose of the one-step prediction of Sigma point set is to estimate the state vector of the  $(k+1)$ -th moment from that of the  $k$ -th moment by using Eq. (6), and then  $\mathbf{Z}_{k+1}^-$  can be calculated by Eq. (9). After that, we calculate the one-step prediction and covariance matrix of the state vector obtained by using weighted summation of the predicted values of the Sigma point set. The weight is obtained by the unscented transformation. The prediction functions are defined

as

$$\begin{aligned}\hat{X}_{k+1}^- &= \sum_{i=0}^{2n} \omega(i) X_{k+1}^-(i) \\ P_{k+1}^- &= \sum_{i=0}^{2n} \omega(i) [\hat{X}_{k+1}^- - X_{k+1}^-(i)] [\hat{X}_{k+1}^- - X_{k+1}^-(i)]^T + Q\end{aligned}\quad (15)$$

where  $\hat{X}_{k+1}^-$  represents the prediction state vector at the time moment  $k+1$ , and  $P_{k+1}^-$  denotes the covariance matrix of the prediction state vector at the time moment  $k+1$ . We then use the unscented transformation again to generate a new set of Sigma points based on the one-step prediction values. The function is defined as

$$X_{k+1}^-(i) = \left[ \hat{X}_{k+1}^- + \sqrt{(n+\lambda)P_{k+1}^-} \hat{\mathbf{e}}_i, \hat{X}_{k+1}^- - \sqrt{(n+\lambda)P_{k+1}^-} \hat{\mathbf{e}}_i \right] \quad (16)$$

We obtain the mean and covariance of the prediction phase by weighted summation based on the predicted observation values of the Sigma point set. The prediction phase functions are defined as

$$\begin{aligned}\bar{Z}_{k+1}^- &= \sum_{i=0}^{2n} \omega(i) Z_{k+1}^-(i) \\ P_{Z_{k+1}Z_{k+1}} &= \sum_{i=0}^{2n} \omega(i) [Z_{k+1}^-(i) - \bar{Z}_{k+1}^-] [Z_{k+1}^-(i) - \bar{Z}_{k+1}^-]^T + R \\ P_{X_{k+1}Z_{k+1}} &= \sum_{i=0}^{2n} \omega(i) [X_{k+1}^-(i) - \hat{X}_{k+1}^-] [Z_{k+1}^-(i) - \bar{Z}_{k+1}^-]^T + R\end{aligned}\quad (17)$$

where  $\bar{Z}_{k+1}^-$  represents the predicted mean of observation function at the time moment  $k+1$ ,  $P_{Z_{k+1}Z_{k+1}}$  and  $P_{X_{k+1}Z_{k+1}}$  represent the state-measurement cross-covariance matrices.  $P_{Z_{k+1}Z_{k+1}}$  denotes the cross-covariance matrix between the predicted observation vector and the predicted mean of observation function.  $P_{X_{k+1}Z_{k+1}}$  denotes the cross-covariance matrix between the predicted state vector and the predicted mean of observation function. The purpose of Eq. (17) is to calculate the mutual covariance matrix of the objective Eq. and the observation Eq., and the mutual covariance matrix integrates the mutual characteristics of the observed value and the estimated value. The Kalman gain is calculated by using the mutual covariance matrix, and the optimal estimation value  $\hat{X}_{k+1}$  of the  $(k+1)$ th moment state vector can be obtained by the Kalman gain.

#### 4.4. Update phase

In the update phase, we calculate the Kalman gain matrix  $K_{k+1}$  and update the state vector and covariance by

$$\begin{aligned}K_{k+1} &= P_{X_{k+1}Z_{k+1}} P_{Z_{k+1}Z_{k+1}}^{-1} \\ \hat{X}_{k+1} &= \hat{X}_{k+1}^- + K_{k+1} [Z_{k+1} - \bar{Z}_{k+1}^-] \\ P_{k+1} &= P_{k+1}^- - K_{k+1} P_{Z_{k+1}Z_{k+1}} K_{k+1}^T\end{aligned}\quad (18)$$

The value of  $\hat{X}_{k+1}$  needs to be modified by nonlinear inequality constraints in Eq. (4) to achieve constraint optimization. We use the maximum angular spread  $\theta_{\max}$  obtained by GBSBSM to constrain the angle of arrival of the mobile base station at different locations. In the NLOS transmission environment, the RSSI measurement value will generate a positive error, so that the measured distance between the mobile base station and the wireless node is greater than the real distance. The objective function and constraint conditions are defined as

$$\begin{aligned}F(x, y) &= \min_{x, y} \left( \left| \alpha_i - \arctan\left(\frac{y_i - y}{x_i - x}\right) \right|^2 + \left| 10^{\frac{\gamma - P(d_i)}{10\epsilon}} - \sqrt{(x_i - x)^2 + (y_i - y)^2} \right|^2 \right) \\ \text{s.t.} \quad &\begin{cases} \arcsin\left(\frac{R_m}{\sqrt{(x_i - x)^2 + (y_i - y)^2}}\right) - \left| \alpha_i - \arctan\left(\frac{y_i - y}{x_i - x}\right) \right| \geq 0 \\ 10^{\frac{\gamma - P(d_i)}{10\epsilon}} - \sqrt{(x_i - x)^2 + (y_i - y)^2} \geq 0 \end{cases}\end{aligned}\quad (19)$$

where  $\alpha_i$  represents the angle of wireless node at the  $i$ -th location detected by the mobile base station. After the optimization process of the nonlinear inequality constraints, new filter update values  $\hat{X}_{k+1}$  and  $P_{k+1}$  are replaced in the next iteration of update state. When NIC-UKF is completed, we can get the position of wireless node from the result of  $\hat{Z}_{k+1}^-$ . The purpose of the constraint conditions is to avoid the filtering divergence of  $\hat{X}_{k+1}$ .

#### 4.5. Curvilinear motion

In the earlier Sections of Section 4, we assume the mobile base station moves in a straight line. But in a real-world environment, a road will not always be a straight line, and there are usually turns or curved roads. Usually, it uses the constant turn rate and the constant tangential acceleration model (CTRA) to model the curvilinear motion [8]. An acceleration



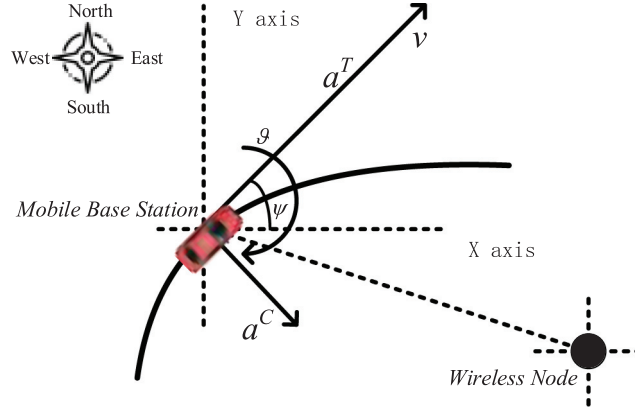


Fig. 4. Curvilinear motion in signal collection.

of curvilinear motion can be decomposed into a tangential acceleration  $\alpha^T$  and a centripetal acceleration  $\alpha^C$ , as shown in Fig. 4. The angles of positions, the speeds, and the accelerations of the mobile base station are defined as

$$\begin{aligned} \psi_{k+1} &= \psi_k + \vartheta_k \cdot t, & v_{k+1} &= v_k + a_k^T \cdot t \\ v_{k+1}^x &= v_{k+1} \cdot \cos(\psi_{k+1}), & v_{k+1}^y &= v_{k+1} \cdot \sin(\psi_{k+1}) \\ a_{k+1}^{T,x} &= a_{k+1}^T \cdot \cos(\psi_{k+1}), & a_{k+1}^{T,y} &= a_{k+1}^T \cdot \sin(\psi_{k+1}) \\ a_{k+1}^{C,x} &= -\vartheta_k \cdot v_{k+1} \cdot \sin(\psi_{k+1}) \\ a_{k+1}^{C,y} &= \vartheta_k \cdot v_{k+1} \cdot \cos(\psi_{k+1}) \end{aligned} \quad (20)$$

where  $t$  is the time interval between two samplings,  $\vartheta$  represents the turn of the mobile base station with a constant rate,  $\psi$  represents the heading angle, and  $v$  represents the velocity of the mobile base station. The superscript  $x$  and  $y$  denote the components in the  $x$  and  $y$  axes respectively.

The Eqs for predicting the location of  $x$  direction and  $y$  direction at the next moment from the previous moment are defined as

$$\begin{aligned} x_{k+1} &= x_k + \frac{v_k \cdot (\sin(\psi_{k+1}) - \sin(\psi_k))}{\vartheta_k} + \frac{a_k^T \cdot (\cos(\psi_{k+1}) - \cos(\psi_k)) + a_k^T \cdot \vartheta_k \cdot t \cdot \sin(\psi_{k+1})}{\vartheta_k^2} \\ y_{k+1} &= y_k - \frac{v_k \cdot (\cos(\psi_{k+1}) - \cos(\psi_k))}{\vartheta_k} + \frac{a_k^T \cdot (\sin(\psi_{k+1}) - \sin(\psi_k)) - a_k^T \cdot \vartheta_k \cdot t \cdot \cos(\psi_{k+1})}{\vartheta_k^2} \end{aligned} \quad (21)$$

We can derive the state vector from the CTra model. The state vector  $X_{ctra}$  is defined as

$$X_{ctra} = (x, v_x, a_x^T, y, v_y, a_y^T, \vartheta) \quad (22)$$

The state-transition matrix is derived as

$$\Phi_{ctra} = \begin{bmatrix} 1 & \frac{\partial x_{k+1}}{\partial v_k^x} & \frac{\partial x_{k+1}}{\partial a_k^{T,x}} & 0 & \frac{\partial x_{k+1}}{\partial v_k^y} & \frac{\partial x_{k+1}}{\partial a_k^{T,y}} & \frac{\partial x_{k+1}}{\partial \vartheta_k} \\ 0 & \frac{\partial v_{k+1}^x}{\partial v_k^x} & \frac{\partial v_{k+1}^x}{\partial a_k^{T,x}} & 0 & \frac{\partial v_{k+1}^x}{\partial v_k^y} & \frac{\partial v_{k+1}^x}{\partial a_k^{T,y}} & \frac{\partial v_{k+1}^x}{\partial \vartheta_k} \\ 0 & 0 & \frac{\partial a_{k+1}^{T,x}}{\partial a_k^{T,x}} & 0 & 0 & \frac{\partial a_{k+1}^{T,x}}{\partial a_k^{T,y}} & \frac{\partial a_{k+1}^{T,x}}{\partial \vartheta_k} \\ 0 & \frac{\partial y_{k+1}}{\partial v_k^x} & \frac{\partial y_{k+1}}{\partial a_k^{T,x}} & 1 & \frac{\partial y_{k+1}}{\partial v_k^y} & \frac{\partial y_{k+1}}{\partial a_k^{T,y}} & \frac{\partial y_{k+1}}{\partial \vartheta_k} \\ 0 & \frac{\partial v_{k+1}^y}{\partial v_k^x} & \frac{\partial v_{k+1}^y}{\partial a_k^{T,x}} & 0 & \frac{\partial v_{k+1}^y}{\partial v_k^y} & \frac{\partial v_{k+1}^y}{\partial a_k^{T,y}} & \frac{\partial v_{k+1}^y}{\partial \vartheta_k} \\ 0 & 0 & \frac{\partial a_{k+1}^{T,y}}{\partial a_k^{T,x}} & 0 & 0 & \frac{\partial a_{k+1}^{T,y}}{\partial a_k^{T,y}} & \frac{\partial a_{k+1}^{T,y}}{\partial \vartheta_k} \\ 0 & 0 & \frac{\partial \vartheta_{k+1}}{\partial a_k^{T,x}} & 0 & 0 & \frac{\partial \vartheta_{k+1}}{\partial a_k^{T,y}} & \frac{\partial \vartheta_{k+1}}{\partial \vartheta_k} \end{bmatrix} \quad (23)$$

In the curvilinear motion, it has the same observation functions as Eq. (9). The noise covariance matrix  $Q_{ctra}$  and  $R_{ctra}$  are defined as

$$Q_{ctra} = \begin{bmatrix} 1 & 0 & 0 & 0 & 0 & 0 & 0 \\ 0 & 1 & 0 & 0 & 0 & 0 & 0 \\ 0 & 0 & 0.1^2 & 0 & 0 & 0 & 0 \\ 0 & 0 & 0 & 0.1^2 & 0 & 0 & 0 \\ 0 & 0 & 0 & 0 & 0.01^2 & 0 & 0 \\ 0 & 0 & 0 & 0 & 0 & 0.01^2 & 0 \\ 0 & 0 & 0 & 0 & 0 & 0 & 0.001^2 \end{bmatrix}, R_{ctra} = \begin{bmatrix} 5^2 & 0 \\ 0 & 0.01^2 \end{bmatrix} \quad (24)$$



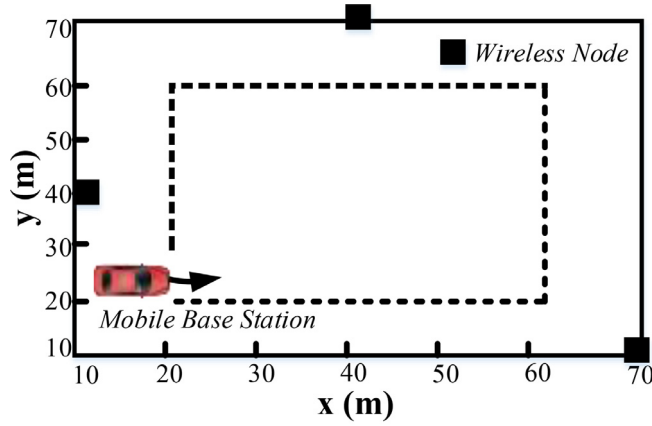


Fig. 5. The localization in a square area.

**Table 1**  
Summary of simulation parameters.

Parameter	Description	Value
$P_T$	signal transmission power	20dBm
$\varepsilon$	path loss exponent	3.68
$PL(d_0)$	path loss constant	41.5dB
$G$	antenna gain	3dBi
$\tau_{\max}$	maximum delay spread	$1.98\mu s$
$\beta$	pending parameter of UT	2
$\lambda = a^2(n + \kappa) - n$	scaling parameter of UT	-5.9994
$W_\sigma$	standard deviation of RSSI noise power	9dBm
$N_{PF}$	number of particles in PF	200
$T$	duration of the trajectory	150s
$\Delta t$	sampling interval	1s
$v$	speed of mobile base station	1m/s

Furthermore, the objective function and constrain conditions of curvilinear motion are as same as those of the linear motion model in Eq. (19).

In order to be suitable for the curvilinear motion, we only need to modify some parameters in the initialization phase of NIC-UKF. We replace the state vector  $\mathbf{X}$ , state-transition matrix  $\Phi$ , noise covariance matrix  $Q$  and  $R$  with  $X_{ctra}$ ,  $\Phi_{ctra}$ ,  $Q_{ctra}$  and  $R_{ctra}$  respectively.

## 5. Experiments and analysis

### 5.1. Simulation experiment

In this section, we design MATLAB simulation experiments to evaluate the performance of the NIC-UKF method on wireless node localization. We consider a representative scenario as shown in Fig. 5. A mobile base station moves along a square track, and there are three wireless nodes deployed along the track.

We assume the locations of the three wireless nodes are [10, 40], [40, 70] and [70, 10] respectively. The velocity of mobile base station is 1m/s in order to be compared with the other research work. Because the base station moves in a uniform linear motion, while the wireless nodes are in a stationary state, in order to describe both of them conveniently, a fixed coordinate system is used to describe their positions. The sampling interval is 1s. The main simulation parameters of ranging model and UT are listed in Table 1.

We use root mean square error (RMSE) to evaluate the performance metric of localization. RMSE is defined as

$$RMSE_t = \sqrt{\frac{1}{n} \sum_{i=1}^n \left[ (x_{i,t} - \hat{x}_{i,t})^2 + (y_{i,t} - \hat{y}_{i,t})^2 \right]} \quad (25)$$

where  $\hat{x}_{i,t}$  denotes the estimate position of actual location  $x_{i,t}$ ,  $n$  denotes the number of sampling points,  $i$  denotes the number of wireless nodes ( $i=1, 2, 3$ ), and  $t$  is the time moment of measure with the maximum value of 150.

In this paper, we use the interior point method which is built in the `fmincon()` function group of MATLAB optimization tools to solve the nonlinear inequality constraint problem in Eq. (16). The processor we used is Inter(R) Core(TM) i7-8750H CPU of 2.20GHz. The memory (RAM) is 16GB, simulation experimental platform is MATLAB. The performance of NIC-UKF

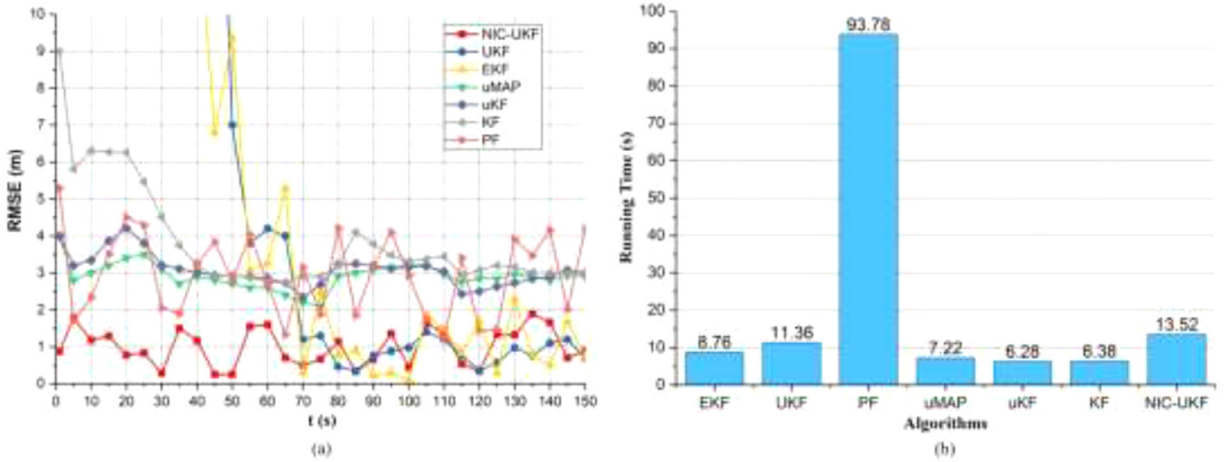


Fig. 6. (a) Experiment results of RMSE (b) Experiment results of time overhead.

is compared with the existing algorithms, such as UKF in [11], EKF in [9], KF in [13], the updated Maximum A Posteriori (uMAP) and the updated Kalman Filter (uKF) in [14], and PF in [12]. The experiment results of the average RMSE is shown in Fig. 6(a). The experiment results of the running time is shown in Fig. 6(b).

From Fig. 6(a), we can observe that the performance of UKF and EKF is mostly better than that of uMAP, uKF and KF. Although uMAP, uKF and KF use the linearization techniques to solve the problem of nonlinear problems, those algorithms ignore the impact of high-order mean and covariance for any nonlinearity. From Fig. 6(a), we see UKF and EKF suffer from significant performance deterioration at the beginning phase of the experiments, but NIC-UKF has a good performance at the beginning phase. It is because we introduce the additional nonlinear inequality constraints, and solve the problem of filtering divergence in UKF and EKF. With the increase of running time, the localization accuracy of most algorithms also increases. It is because most filtering algorithms are based on iterative computation, and the number of iterations affects the filtering performance. Fig. 6(a) shows NIC-UKF has the best stability and fast convergence time.

In Fig. 6(b), we can observe that PF has the longest running time. PF uses a number of particles, which increases computational complexity. Note that NIC-UKF has the second longest running time. It is because NIC-UKF needs to modify the value of  $\hat{x}_{i,t}$  by nonlinear inequality constraints to achieve the effect of constraint optimization in each iteration after UKF. Although it costs a little longer running time, it is acceptable to use NIC-UKF. We can deploy a mobile base station with powerful computing power or upload the collecting data to a cloud server to improve the computing speed because the volume of collecting data are small.

## 5.2. Reality experiment

In this experiment, we deployed eight wireless sensor nodes in the campus of University of Technology Sydney. In order to measure in a normal manner, we chose forty measurement positions with uniform space on the road. During a round measurement, the five nodes with the nearest spherical distance from the base station were measured. At the same time, nodes were deployed at different locations with different density to verify the localization results in the actual environment. We measured the actual RSSI values in NLOS environment to avoid interference from obstacles. The scenario of RSSI measure is shown in Fig. 7.

We apply nonlinear inequality constraints in Eq. (19) to restrict the perturbation under the impact of NLOS. In this experiment, the locations of the wireless nodes and the marked points (Points whose positions are known in advance) are known. We add some positive errors with Gaussian distribution to the actual RSSI values. The standard deviation of RSSI noise power is 9dBm. After being processed by the interior point method in Eq. (19), we can get the results of revised RSSI values. In Fig. 8(a), the revised RSSI values are compared with the values of actual RSSI and the RSSI with errors. We compute the estimated distance between each marked point and the corresponding sensor nodes by using the log-distance path loss model. The parameters of Eq. (2) are listed in Table 1 in Section 5.1. The estimated distance of actual RSSI, RSSI with errors and revised RSSI are shown in Fig. 8(b) respectively.

From Fig. 8(a), we can observe that the polyline of revised RSSI fits well with that of actual RSSI. That is to say, NIC-UKF can effectively eliminate NLOS errors. However, we can observe that there are inaccuracy prediction values in marked points 7, 13, 26 and 36. In addition, those marked points appear on vertexes of polylines. In other words, the performance of NIC-UKF will decline in the moments of RSS fluctuation. It is because of the incorrectly prediction of the ranging model when RSS fluctuates. One way to solve RSS fluctuation is to use smoothing filtering to take into account the values around the RSSI values measured at a certain time.



Fig. 7. The scenario of RSSI measure.

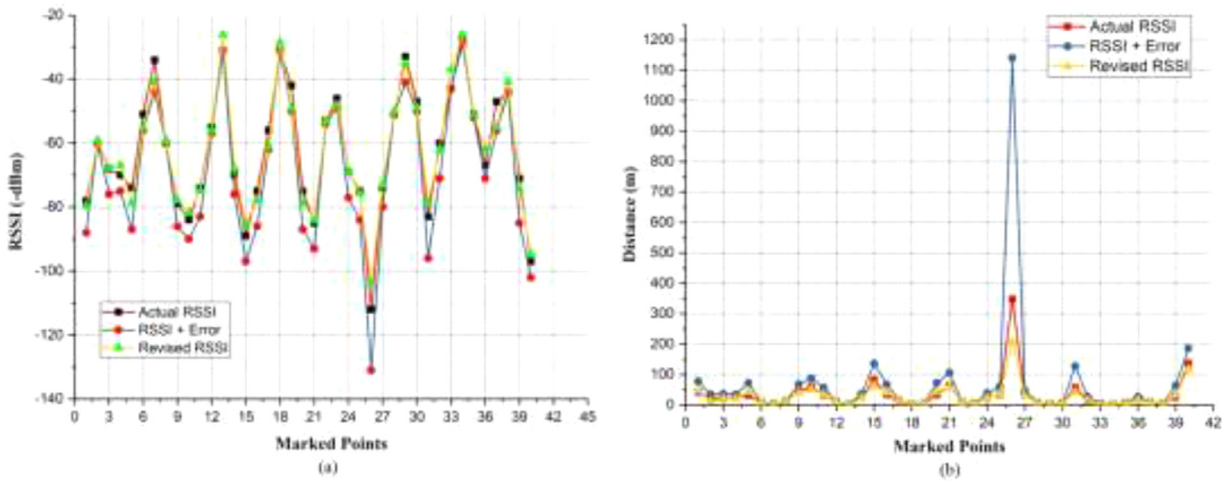


Fig. 8. (a) Comparison of RSSI values (b) Comparison of estimated distance.

In Fig. 8(b), we can observe that there is an obvious misestimation of distance in the marked point 26. The value of actual RSSI is  $-112\text{dBm}$ , while the value of RSSI with errors is  $-131\text{dBm}$  respectively. Eventually, the estimated distance of actual RSSI is  $347.34\text{m}$ , but the estimated distance of RSSI with errors is  $1140.42\text{m}$ . It is because the estimated distance has the exponential relation with the signal strength in the log-distance path loss model. A little error will cause a serious misestimation. Therefore, it is necessary to add constraints with the filtering approaches. Furthermore, we can predict the locations of obstacles based on the estimated distance. If there is a serious error of estimated distance, we can draw a conclusion that there are obstacles within line of sight propagation.

## 6. Conclusions and future work

In this paper, a nonlinear inequality constrained-unscented Kalman filter method is provided to address the localization problem of wireless nodes under the non-line of sight. The contributions of this paper include it introduces the angle and distance constraints to the unscented Kalman filter, and improves the convergence speed and localization accuracy with acceptable computation consumption. The nonlinear inequality constrained-unscented Kalman filter method includes four phases, i.e., the initialization phase, the unscented transformation phase, the prediction phase, and the update phase. The idea of the nonlinear inequality constrained-unscented Kalman filter method is to remove the interference of noise through the observation and prediction of its positions and the received signals during the base station motion. We can obtain the signal strength without interference in the update phase. After that, the real distance of wireless nodes can be calculated according to the signal propagation model. The nonlinear inequality constrained-unscented Kalman filter method is suitable for the localization of wireless nodes based on angles of arrival and received signal strength indications under the non-line of sight when a base station is in the linear motion or the curvilinear motion.

In the simulation experiment, we compared the localization accuracy and calculation time overhead between the nonlinear inequality constrained-unscented Kalman filter and the extended Kalman filter, the unscented Kalman filter, the particle filter, the updated maximum a posteriori, the updated Kalman filter and the Kalman filter. The experimental results show that the nonlinear inequality constrained-unscented Kalman filter has the advantages of faster convergence speed, high localization accuracy, better stability, and acceptable running time. In the real experiment, we evaluate the effect of the nonlinear inequality constrained-unscented Kalman filter on noise filtering, and the experimental results show that the nonlinear inequality constrained-unscented Kalman filter has good noise filtering effect, and can be used to localize the positions of wireless nodes accurately.

In the future work, we will consider the energy optimization during signal collection in order to reduce the energy consumption of the mobile base station.

## Declaration of Competing Interest

The authors declare that they have no known competing financial interests or personal relationships that could have appeared to influence the work reported in this paper.

## Acknowledgements

This work is supported by the [National Natural Science Foundation of China](#) under Grants No. 61572164, No. 61572160, No. 61877015, No. 61850410531, No. 61602137, No. 61402417, No. 61473109 and No. 61472112, [Zhejiang Provincial Natural Science Foundation](#) under Grants No. LY19F020016 and No. LY19F020044, the Reform Project of Higher Education in Zhejiang under Grants No. jg20160071, and the project of education planning in Zhejiang under Grants No. 2018SCG005.

## Supplementary materials

Supplementary material associated with this article can be found, in the online version, at doi:[10.1016/j.compeleceng.2020.106694](https://doi.org/10.1016/j.compeleceng.2020.106694).

## References

- [1] Rajkumar R, Lee I, Sha L, Stankovic J. Cyber-physical systems: the next computing revolution. In: 2010 47th ACM/IEEE design automation conference (DAC). IEEE; 2010. p. 731–6.
- [2] Zhou X, Liang W, Wang K, Huang R, Jin Q. Academic influence aware and multidimensional network analysis for research collaboration navigation based on scholarly big data. *IEEE Trans Emerg Topics Comput* 2018. doi:10.1109/TETC.2018.2860051.
- [3] Zhou X, Wu B, Jin Q. Analysis of user network and correlation for community discovery based on topic-aware similarity and behavioral influence. *IEEE Trans Human-Mach Syst* 2018;48(6):559–71.
- [4] Huang C, Marshall J, Wang D, Dong M. Towards reliable social sensing in cyber-physical-social systems. In: 2016 IEEE international parallel and distributed processing symposium workshops (IPDPS). IEEE; 2016. p. 1796–802.
- [5] Zhou Y, Ao X, Xia S. An improved APIT node self-localization algorithm in WSN. In: 2008 7th world congress on intelligent control and automation (WCICA). IEEE; 2008. p. 7582–6.
- [6] Guvenc I, Chong CC. A survey on TOA based wireless localization and NLOS mitigation techniques. *IEEE Commun Surv Tutor* 2009;11(3):107–24.
- [7] Le BL, Ahmed K, Tsuji H. Mobile location estimator with NLOS mitigation using kalman filtering. In: 2013 IEEE wireless communications and networking (WCNC). IEEE; 2013. p. 1969–73.
- [8] Zhang M, Wang J, Ji Z. A novel algorithm of NLOS error mitigation based on kalman filter in cellular wireless location. In: 2009 5th International conference on wireless communications, networking and mobile computing (WiCOM). IEEE; 2009. p. 1–4.
- [9] Yang S, Li H. Application of EKF and UKF in target tracking problem. In: 2016 8th International conference on intelligent human-machine systems and cybernetics (IHMSC). IEEE; 2016. p. 116–20.
- [10] Hammes U, Wolsztynski E, Zoubir AM. Robust tracking and geolocation for wireless networks in NLOS environments. *IEEE J. Select Topics Signal Proc* 2009;3(5):889–901.
- [11] Nowak T, Eidloth A. Dynamic multipath mitigation applying unscented kalman filters in local positioning systems. *Int J Microwave Wireless Technol* 2011;3(03):365–72.
- [12] Read J, Achutegui K, Míguez J. A distributed particle filter for nonlinear tracking in wireless sensor networks. *Signal Process* 2014;98:121–34.
- [13] Khan MW, Kemp AH, Salman N, Mihaylova L. Tracking of wireless mobile nodes in the presence of unknown path-loss characteristics. In: 2015 18th international conference on information fusion (FUSION). IEEE; 2015. p. 104–11.
- [14] Tomic S, Beko M, Dinis R, Gomes J. Target tracking with sensor navigation using coupled RSS and AoA measurements. *Sensors* 2017;17(11):2690.
- [15] Wang J, Urriza P, Han Y, Cabric D. Weighted centroid localization algorithm: Theoretical analysis and distributed implementation. *IEEE Trans Wireless Commun* 2011;10(10):3403–13.
- [16] Sun X, Chen T, Li W, Zheng M. Performance research of improved MDS-MAP algorithm in wireless sensor networks localization. In: 2012 international conference on computer science and electronics engineering (CSEE). IEEE; 2012. p. 587–90.
- [17] Xu B, Sun G, Yu R, Yang Z. High-accuracy TDOA-based localization without time synchronization. *IEEE Trans Parallel Distrib Syst* 2013;24(8):1567–76.
- [18] Leng YF, Zhu HP, Alsharari T, He F. An improved RSSI positioning algorithm based on reference distances. *Adv Mater Res* 2014;971:1547–52.
- [19] Pradhan S, Shin S, Kwon GR, Pyun JY, Hwang SS. The advanced TOA trilateration algorithms with performance analysis. In: 2016 50th asilomar conference on signals, systems and computers (ASILOMAR). IEEE; 2016. p. 923–8.
- [20] Zhang R, Liu J, Du X, Li B, Guizani M. AOA-based three-dimensional multi-target localization in industrial WSNs for LOS conditions. *Sensors* 2018;18(8):2727.
- [21] Li J, Zhang J, Liu X. A weighted dv-hop localization scheme for wireless sensor networks. In: 2009 international conference on scalable computing and communications & 8th international conference on embedded computing (scalcom-embeddedCom). IEEE; 2009. p. 269–72.
- [22] Rappaport TS. Wireless communications: principles and practice. *Microwave J* 2002;45(12):128–9.
- [23] Parsons JD, Parsons PJ. The mobile radio propagation channel. Wiley; 1992.

**Zhigang Gao** is an associate professor in Hangzhou Dianzi University. He received the Ph.D. degree from Zhejiang University, China in 2008. His current research interests include mobile computing and Cyber-Physical Systems.

**Hongyi Guo** is a graduate student at Hangzhou Dianzi University. He received his BS in computer science and technology from Henan University, China. His research interest is computer architecture.

**Yunfeng Xie** is a graduate student at Hangzhou Dianzi University. He received his BS in computer science and technology from Henan University, China. His research interest is mobile computing.

**Huijuan Lu** is a professor in China Jiliang University. She received Ph.D. degree from China University of Mining and Technology. Her research interests include mobile computing and artificial intelligence.

**Jianhui Zhang** is a professor in Hangzhou Dianzi University. He received his Ph.D. from Zhejiang University, Hangzhou, China in 2008. He is the leader of the IoT group. His research interests include IoT, energy-harvesting micro-systems and networking, algorithm designing and applications, and crowdsourcing.

**Wenjie Diao** received the B.S. degree in network engineering from Fujian University of Technology. He is currently pursuing a M.S. degree in Computer Technology in Hangzhou Dianzi University. His interests include mobile computing, mobile phone security, neural networks and so on.

**Ruichao Xu** received the B.S. degree in digital media technology from Anhui University of Science and Technology. He is currently pursuing a M.S. degree in computer science and technology from Hangzhou Dianzi University. His research interests include mobile computing, security scheduling, and big data.